Available online at www.sciencedirect.com
ScienceDirect
Journal of Molecular Catalysis A: Chemical 278 (2007) 237–243
JOURNAL OF MOLECULAR CATALYSIS A: CHEMICAL
www.elsevier.com/locate/molcata

An active La/TiO_2 photocatalyst prepared by ultrasonication-assisted sol–gel method followed by treatment under supercritical conditions

Yuning Huo, Jian Zhu, Jingxia Li, Guisheng Li, Hexing Li *

Department of Chemistry, Shanghai Normal University, Shanghai 200234, PR China

Received 13 June 2007; received in revised form 16 July 2007; accepted 29 July 2007
Available online 19 August 2007

Abstract

A La-doped TiO_2(La/TiO_2) photocatalyst with optimum La/Ti molar ratio of 1.25% is prepared by ultrasound-assisted sol–gel method, followed by supercritical drying in ethanol fluid. During liquid phase photocatalytic degradation of phenol, the as-prepared La/TiO_2 exhibits higher activity than the La/TiO_2 obtained without ultrasonication. Meanwhile, the La/TiO_2 obtained via supercritical treatment is more active than either the undoped TiO_2 obtained under supercritical conditions or the La/TiO_2 obtained via direct calcination instead of supercritical treatment. Based on various characterizations, the promoting effects of ultrasonication, supercritical treatment, and La-modification are discussed by considering the enhanced particle dispersion, the higher crystallization degree of anatase and the increase of the surface oxygen vacancies and/or defects, which facilitates the adsorption of phenol molecules and also inhibits the recombination between photoelectrons and holes, resulting in the higher quantum efficiency of photocatalysis. Meanwhile, the ultrasonication and supercritical treatment also strengthen the interaction between the La-dopants and the TiO_2, which could enhance the light absorbance and thus, increase the photocatalytic activity.

Keywords: La-doped TiO_2 photocatalyst; Ultrasonication; Supercritical treatment; Phenol degradation

1. Introduction

Photocatalysis attracts considerable attentions owing to its potential in environmental cleaning [1]. Most studies have involved the TiO_2-based photocatalysts owing to the cheapness, stability, nontoxicity and environmental friendship [2–4]. However, the pure TiO_2 usually shows low quantum efficiency due to the recombination of photo-induced electrons and holes. Many attempts have been made to achieve high activity by doping the TiO_2 with metal particles, metallic ions, nonmetallic ions, and other semiconductor oxides [5–9]. La compounds are easily obtained and it has been proved that modification of TiO_2 with La-dopants shows significant improvement on both the photocatalytic activity and the thermal stability [10–13]. To date, nearly all the La-doped TiO_2 photocatalysts are synthesized by sol–gel method, followed by calcination to strengthen the incorporation between the La-dopants and the TiO_2 and to enhance the crystallization degree of anatase. However, calcinations at high temperature usually cause particle agglomeration and pore collapse, leading to the low surface area and the poor dispersion of the La-dopants in the TiO_2 network which is harmful for photocatalytic activity [14–16]. Previously, we reported a new approach to synthesize TiO_2-based photocatalysts via supercritical treatment [17–19]. The absence of surface tension under supercritical conditions leads to preservation of the porous structure in the precursors during calcinations, corresponding to the high surface area. Meanwhile, the very high pressure and local temperature under supercritical conditions ensure strong incorporation of the dopants into TiO_2 network. Up to now, the N-, S-, and SO_4^{2-}-doped TiO_2 photocatalysts have been synthesized under supercritical conditions which show higher activity than the corresponding ones obtained via direct calcinations instead of supercritical treatment. Besides, the application of ultrasonication in preparation of TiO_2 photocatalysts has been recently developed by Yu et al. [20,21]. In this paper, as a continuation of our researching work, we report the preparation of a La-doped TiO_2(La/TiO_2) photocatalyst via ultrasound-assisted sol–gel method, followed by supercritical treatment. The promoting effects of both the La-doping and the supercritical treatment

* Corresponding author. Tel.: +86 21 6432 2142; fax: +86 21 64322272.
E-mail address: HeXing-Li@shnu.edu.cn (H. Li).

1381-1169/$ – see front matter © 2007 Elsevier B.V. All rights reserved.
doi:10.1016/j.molcata.2007.07.054

as well as the ultrasonication are discussed briefly based on a detailed characterizations.

2. Experimental

2.1. Catalyst preparation

A solution containing desired amount of $La(NO_3)_3$, 2.5 ml (1:5, v/v) HNO_3 and 10 ml alcohol (EtOH) is added dropwise into the solution containing 10 ml $Ti(O–C_4H_9)_4$ and 40 ml EtOH at 313 K under vigorous stirring, which is allowed to hydrolyze under 100 W 60 kHz ultrasonic irradiation (JY88-II). After being aged for 48 h at 313 K, the xerogel is transferred into 500 ml autoclave containing 250 ml EtOH and is treated under supercritical conditions (553 K and 11.5 MPa) for 2 h. Then, the vapor inside the autoclave is released slowly and the system is cooled down to room temperature in the N_2 flow. The as-received solid is calcined for 8 h at given temperature to remove the residual organic compounds and solvent. The optimum calcination temperature is determined as 773 K. The La-content in the La/TiO_2 sample could be adjusted by changing the $La(NO_3)_3$ concentration in the mother solution. The as-prepared samples are denoted as La/TiO_2-*x*(SC/US), where SC, US and *x* represent the supercritical treatment, the ultrasonication, and the La/Ti molar ratio, respectively. For comparison, the La-doped TiO_2 samples are also prepared by sol–gel method without ultrasonication and/or supercritical treatment, and are denoted as La/TiO_2-*x*(DC) and La/TiO_2-*x*(SC) where DC refers to the direct calcination.

2.2. Catalyst characterization

The structure of the as-prepared samples is determined by both X-ray diffraction (XRD, Rigacu Dmax-3C, Cu Kα radiation) and FTIR (NEXUS 470) as well as Raman spectra (Super Labram). Transmission electronic micrograph (TEM, JEM-2010) is employed to observe the surface morphology. The N_2 adsorption–desorption isotherms are obtained by on a NOVA 4000 at 77 K, from which the surface area (S_{BET}), the pore volume (V_P) and the pore diameter (d_P) are calculated by BET and BJH methods, respectively. The light absorption is detected by photoluminescence spectra (PLS, Varian Cary-Eclipse 500) and UV–vis diffuse reflectance spectra (DRS, MC-2530).

2.3. Activity test

The phenol degradation is carried out at 303 K in a self-designed glassy reactor containing 0.050 g catalyst, and 30 ml 0.1 g/l phenol aqueous solution. The reaction mixture is stirred vigorously (>1000 rpm) to eliminate the diffusion effect. After reaching adsorption equilibrium, the photocatalysis is initiated by irradiating the system with three 8 W lamps (characteristic wavelength of 310 nm). Each run of the reaction is lasted for 4 h and the phenol left in the solution is analyzed by a UV spectrophotometer (UV 7504/PC) at the characteristic wavelength ($\lambda = 270$ nm), from which the phenol degradation yield is calculated. Preliminary tests confirm a good linear relationship between the light absorbance at 270 nm and the phenol concentration. Meanwhile, blank experiments also demonstrate that only less than 3% phenol decomposed after reaction for 4 h in the absence of either the photocatalyst or the UV light irradiation and thus could be neglected in comparison with the phenol degradation yield through photocatalysis. The GC and HPLC analyses demonstrate that, besides carbon dioxide, the intermediates produced during the photocatalysis could be neglected after the phenol degradation yield reaches more than 30%, showing the complete mineralization of phenol under present conditions. The reproducibility of the results is checked by repeating the results at least three times and was found to be within acceptable limits (±5%).

3. Results and discussion

3.1. Structural characteristics

The FTIR spectra (Fig. 1) demonstrate that, besides of the absorption peaks at 1630 and 3400 cm^{-1} indicative of the Ti–O bonding and the surface OH group was found in undoped TiO_2(SC) [16], both the La/TiO_2-1.25(SC) and the La/TiO_2-1.25(SC/US) samples display an absorption peak around 510 cm^{-1} characteristic of the La–O bond [22], showing the successful incorporation of the La-dopants with the TiO_2, which are mainly present in oxides. The XPS spectra in Fig. 2 confirm that all the La species are present in the form of La_2O_3, corresponding to the binding energies of 835.5 and 852.3 eV in the La $3d_{5/2}$ and La $3d_{3/2}$ levels, respectively.

Fig. 3 shows the TEM morphologies of the undoped and La-doped TiO_2 samples obtained via different methods. The La/TiO_2(SC) shows more homogeneous particle distribution than either the undoped TiO_2(SC) or the La/TiO_2(DC), indicating that both the La-doping and the supercritical treatment instead of direct calcination could effectively inhibit the agglomeration of the TiO_2 nanoparticles. The particles in the La/TiO_2(SC/US) are even more homogeneous owing to the dispersing role of ultrasonication. Considering the particle shape, it is found that La/TiO_2-1.25(DC) is comprised of

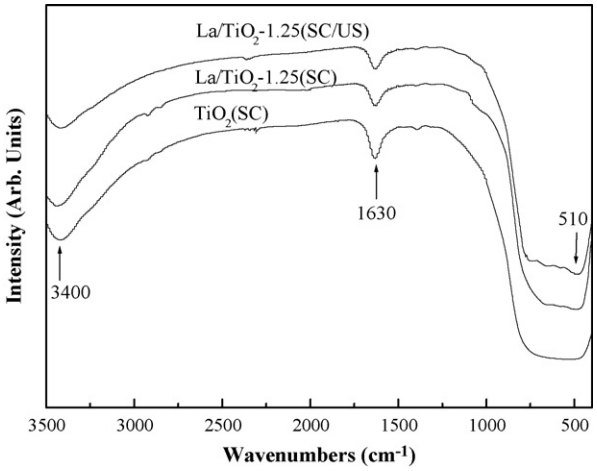

Fig. 1. FTIR spectra of TiO_2(SC), La/TiO_2-1.25(SC), and La/TiO_2-1.25(SC/US) samples.

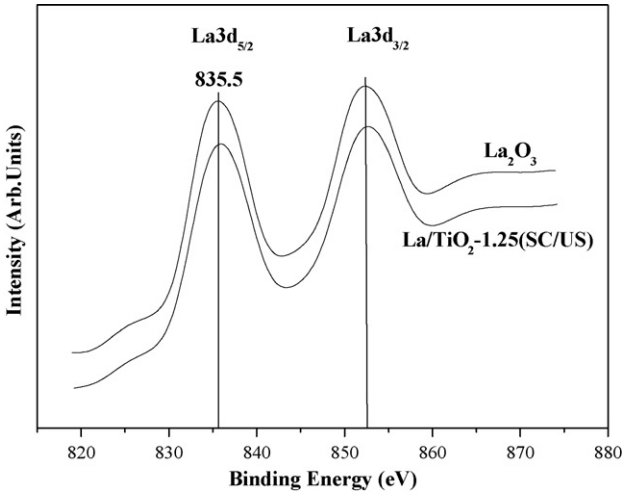

Fig. 2. XPS spectra of La_2O_3 and La/TiO_2-1.25(SC/US) samples.

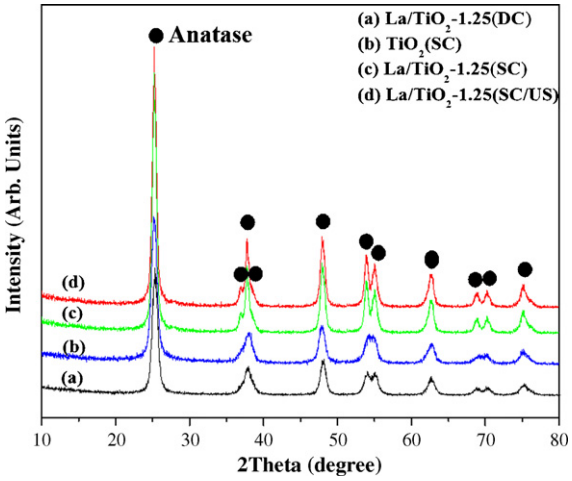

Fig. 4. XRD patterns of (a) La/TiO_2-1.25(DC), (b) TiO_2(SC), (c) La/TiO_2-1.25(SC), and (d) La/TiO_2-1.25(SC/US) samples calcined at 773 K.

spherical nanoparticles while all the other samples obtained via supercritical treatment, i.e., TiO_2(SC), La/TiO_2-1.25(SC) and La/TiO_2-1.25(SC/US), are present in the cubic nanoparticles. Taking into account of the cubic crystal lattice of anatase, one could conclude that the supercritical treatment promotes the crystallization of anatase. The attached SAED and HRTEM images show that all the samples are present in crystalline anatase after being calcined at 773 K for 8 h, but the La/TiO_2-1.25(SC) and the La/TiO_2-1.25(SC/US) display high crystallization degree which is further confirmed by XRD patterns. As shown in Fig. 4, both the La/TiO_2-1.25(SC) and the La/TiO_2-1.25(SC/US) display more distinguished peaks indicative of anatase phase with extensive intensity than either the TiO_2(SC) or the La/TiO_2-1.25(DC), implying that the La-doping

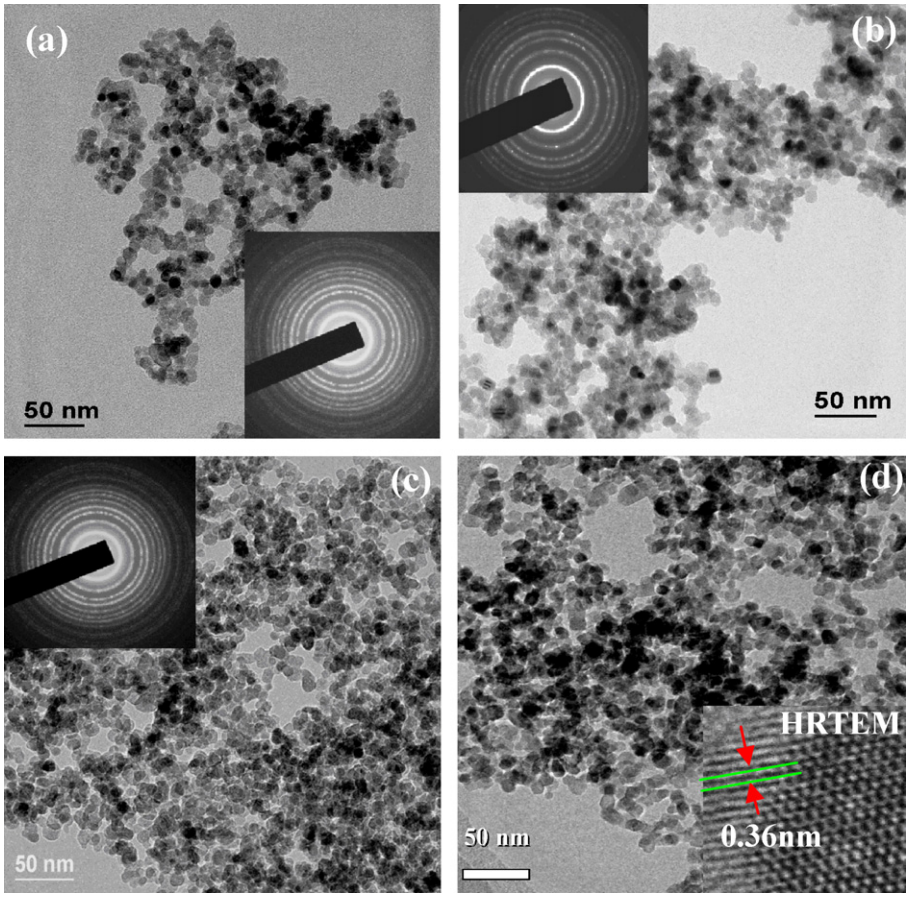

Fig. 3. TEM morphologies of (a) TiO_2(SC), (b) La/TiO_2-1.25(DC), (c) La/TiO_2-1.25(SC), and (d) La/TiO_2-1.25(SC/US) samples calcined at 773 K. The attached are the SAED and HRTEM images.

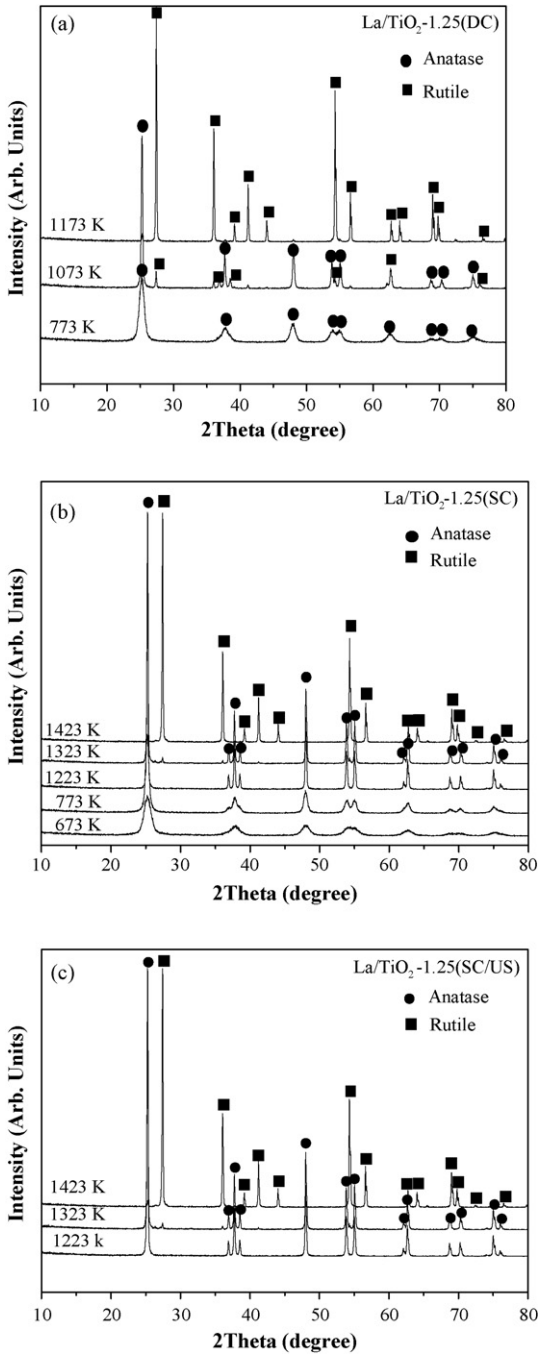

Fig. 5. XRD patterns of (a) La/TiO_2-1.25(DC), (b) La/TiO_2-1.25(SC), and (c) La/TiO_2-1.25(SC/US) samples calcined at elevated temperatures.

and the supercritical treatment lead to the increase of crystallization degree of anatase. The La/TiO_2-1.25(SC/US) exhibits a similar XRD pattern to the La/TiO_2-1.25(SC), suggesting that the ultrasonic irradiation has no significant influence on the crystallization degree.

Fig. 5 reveals that the crystallization degree of anatase increased with the increase of calcination temperature. Both the La/TiO_2-1.25(SC) and the La/TiO_2-1.25(SC/US) remain their anatase phase until being calcined at 1223 K. However, the La/TiO_2-1.25(DC) sample displays transformation from anatase to rutile at 1073 K. We previously reported that the rutile phase appears in the TiO_2(SC) after being calcined at 1023 K [17]. The higher thermal stability of the La/TiO_2-1.25(SC) than that of the TiO_2(SC) demonstrates the stabilizing effect of the La-dopants on the anatase since the coverage of the TiO_2 surface by La_2O_3 species could protect the TiO_2 nanoparticles from agglomeration during calcinations. Meanwhile, partial La_2O_3 species incorporate into the TiO_2 network might enhance the straining force in the anatase lattice due to structural distortion, which could further inhibit the phase transformation from anatase to rutile. The La/TiO_2-1.25(SC) exhibits much higher thermal stability than the La/TiO_2-1.25(DC) owing to the presence of porous structure in the TiO_2 sample which might inhibit particle gathering. Besides, the supercritical treatment might strengthen the interaction between the La-dopants and the TiO_2 network, leading to enhanced thermal stability since the phase change from anatase to rutile during calcinations is effectively inhibited. No speaks indicative of the anatase crystallization phase have been observed in the XRD patterns even after being calcined at very high temperature, possibly due to the low La-content and the high dispersion of the La-dopants in all the La/TiO_2 samples.

The Raman spectra in Fig. 6 demonstrate that all the samples calcined at 773 K are present in pure anatase phase corresponding to the characteristic peaks around 142, 394, 514, 638 cm^{-1}, respectively [23]. The La-doping causes a slight blue shift of the principal peak and the ultrasonication leads to further blue shift, showing the increase of oxygen vacancies [24], which could be attributed to the distortion of anatase crystalline lattice induced by La-doping. The attached Raman spectra demonstrate that the increase of the calcination temperature results in a slight red shift of the principal peak in the La/TiO_2-1.25(SC/US), implying the decrease oxygen vacancies which could be attributed to the enhanced crystallization degree of anatase.

As shown in Fig. 7, the PLS spectra display an absorbance peak around 382 nm for both the undoped and La-doped TiO_2 samples, corresponding to the emission peak from band edge free excitation. The intensity of the peak around 382 nm increases in the order of La/TiO_2-1.25(DC), TiO_2(SC),

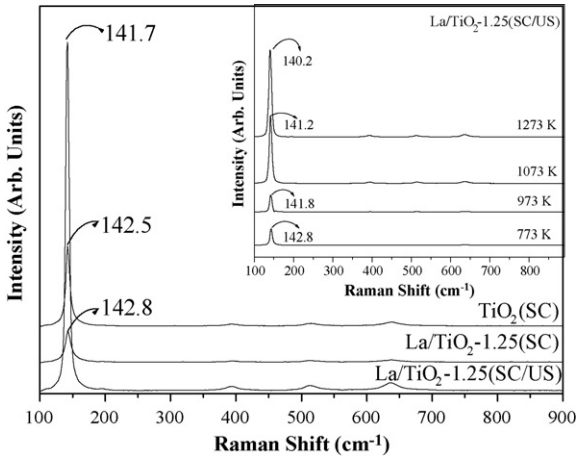

Fig. 6. Raman spectra of TiO_2(SC), La/TiO_2-1.25(SC) and La/TiO_2-1.25(SC/US) samples calcined at 773 K. The attached is Raman spectra of the La/TiO_2-1.25(SC/US) calcined at elevated temperature.

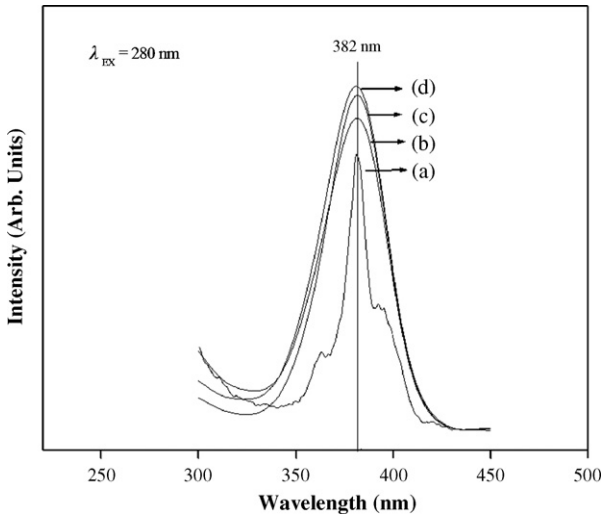

Fig. 7. PLS spectra of (a) La/TiO_2-1.25(DC), (b) TiO_2(SC), (c) La/TiO_2-1.25(SC), and (c) La/TiO_2-1.25 (SC/US) samples calcined at 773 K.

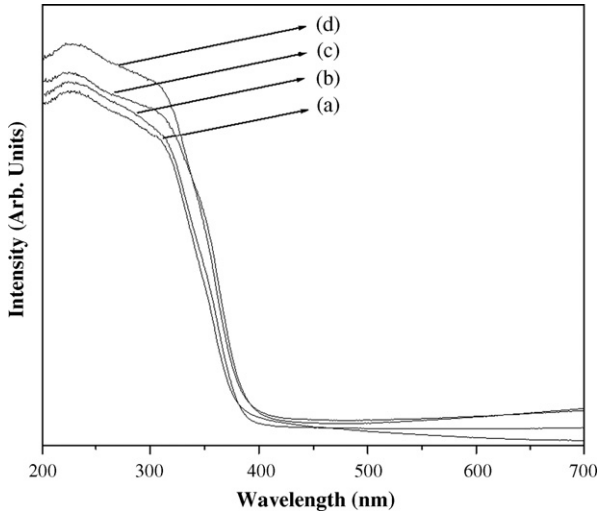

Fig. 8. UV–vis DRS spectra of (a) TiO_2(SC), (b) La/TiO_2-1.25(DC), (c) La/TiO_2-1.25(SC), and (d) La/TiO_2-1.25(SC/US) calcined at 773 K.

La/TiO_2-1.25(SC), and La/TiO_2-1.25(SC/US), indicating that the La-doping, the supercritical treatment and the ultrasonication could increase oxygen vacancies and/or surface defects in the TiO_2 photocatalysts [25], which is consistent with the results from aforementioned Raman spectra. Meanwhile, the UV–vis DRS spectra (Fig. 8) display enhanced ability for UV light absorbance in the order of TiO_2(SC), La/TiO_2-1.25(DC), La/TiO_2-1.25(SC), and La/TiO_2-1.25(SC/US), showing the promoting effect of the La-doping, the supercritical treatment and the ultrasonication on the light absorbance.

Other structural parameters are listed in Table 1. The La/TiO_2-1.25(SC) exhibits much higher S_{BET} than either the TiO_2(SC) or the La/TiO_2-1.25(DC). On one hand, treatment under supercritical conditions could preserve the porous structure existed in the TiO_2 xerogel precursor owing to the lack of surface tension, resulting in the larger V_P and D_P which could account for the higher S_{BET} of the La/TiO_2-1.25(SC) than that of the La/TiO_2-1.25(DC). On the other hand, the La-doping could enhance the particle dispersion [10], as confirmed by TEM morphologies in Fig. 3. Meanwhile, more micropores might be created owing to the incorporation of the La_2O_3 into the TiO_2 network, corresponding to the increase in V_P but the decrease in D_P. These results could account for the higher S_{BET} of the La/TiO_2-1.25(SC) than that of the La/TiO_2-1.25(DC). Comparing the La/TiO_2-1.25(SC) and the La/TiO_2-1.25(SC/US), one could see that the ultrasonication could further enhance the S_{BET}, possibly owing to increase of particle dispersion degree [26] and the presence of more micropores in the La/TiO_2-1.25(SC/US), which could be attributed to the bubbles arisen from acoustic cavitation [27,28]. The presence of more micropores could also account for larger V_P but lower D_P of the La/TiO_2-1.25(SC/US) comparing to the La/TiO_2-1.25(SC). Increase of the calcination temperature from 773 to 973 K results in a slight decrease in S_{BET} due to the particle gathering. Further increase in the calcination temperature to 1173 K leads to an abrupt decrease in the S_{BET}, possibly due to the collapse of porous structure, corresponding to the abrupt decrease in V_P.

3.2. Catalytic performance

The photocatalytic degradation of phenol is employed as a probe to examine the catalytic performances of the as-prepared undoped and La-doped TiO_2 samples. Besides CO_2, no other products have been identified during the reaction, suggesting

Table 1
Some structural parameters of the TiO_2 and La-doped TiO_2 samples

Sample	Calcination temperature (K)	S_{BET} (m^2/g)	V_p (cm^3/g)	d_P (nm)	Degradation (%)
P25	773	45	0.25	20	38
TiO_2(SC)	773	68	0.37	20	57
La/TiO_2-1.25(DC)	773	86	0.11	5.0	56
La/TiO_2-1.25(SC)	673	141	0.50	15	52
La/TiO_2-1.25(SC)	773	139	0.51	15	68
La/TiO_2-1.25(SC)	973	126	0.49	16	61
La/TiO_2-1.25(SC)	1173	54	0.13	9.0	31
La/TiO_2-1.25(SC/US)	773	153	0.99	8.2	73

Reaction conditions: 0.050 g photocatalyst, 30 ml 0.10 g/l phenol aqueous solution, three 8 W lamps (310 nm) at 4 cm above the reaction solution, reaction temperature = 303 K, stirring rate = 1000 rpm, reaction period = 4 h.

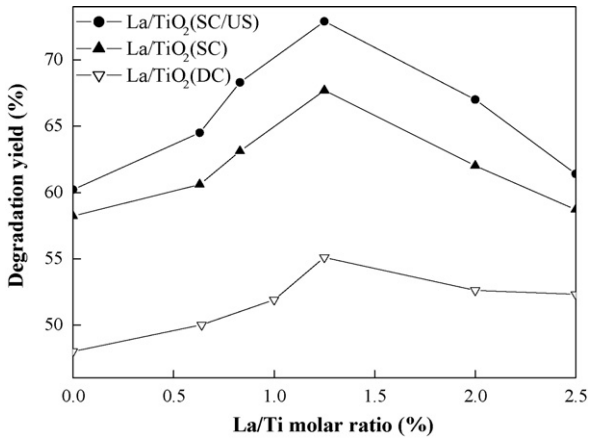

Fig. 9. Dependence of the activity on the La-content. *Reaction conditions*: 0.050 g La/TiO_2 photocatalyst calcined at 773 K, 30 ml 0.10 g/l phenol aqueous solution, three 8 W lamps (310 nm) at 4 cm above the reaction solution, reaction temperature = 303 K, stirring rate = 1000 rpm, reaction period = 4 h.

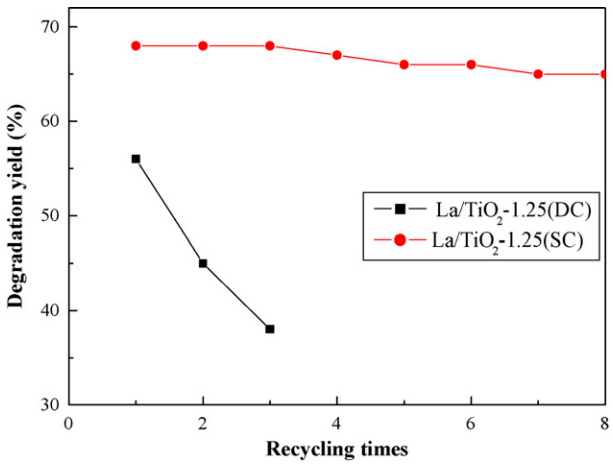

Fig. 10. Durability test of the La/TiO_2-1.25(DC) and the La/TiO_2-1.25(SC) photocatalysts. Reaction conditions are given in Fig. 9.

the complete phenol mineralization under the present conditions. Fig. 9 reveals that the activity first increases and then decreases with the La-content. The optimum La/Ti molar ratio is determined as 1.25% for all the as-prepared La-doped TiO_2 photocatalysts. From the phenol degradation yields listed in Table 1, the following results can be drawn.

(1) The La/TiO_2-1.25(SC) exhibits much higher activity than the TiO_2(SC), showing the promoting effect of the La-modification. On one hand, the La-modification increases the S_{BET} (see Table 1), which facilitates the adsorption for phenol molecules. On the other hand, the La-modification could enhance the crystallization degree of the anatase (see Fig. 4), which favors the transfer and the separation of photo-induced electrons and holes to prevent from their recombination, leading to the enhanced quantum efficiency. Meanwhile, the La-modification could increase the oxygen vacancies and/or surface defects in the TiO_2 photocatalysts which might capture photoelectrons and thus, inhibit the recombination between photoelectrons and holes, resulting in enhanced quantum efficiency. Furthermore, the La-modification could enhance the absorbance for UV lights, which could generate more photo-induced holes served as active sites for phenol degradation. However, as shown in Fig. 9, very high La-content is harmful for the photocatalytic activity due to the great coverage of the TiO_2 surface by La_2O_3 species, taking into account that the TiO_2 serves as active sites for photocatalysis.

(2) The La/TiO_2-1.25(SC) shows higher activity than the La/TiO_2-1.25(DC), indicating the promoting effect of the supercritical treatment which has been discussed in our previous papers [17–19]. Briefly, the La/TiO_2-1.25(SC) obtained under supercritical conditions has high surface area and large pore volume owing to the reservation of porous structure originally present in the xerogel precursor, which facilitates the adsorption for phenol molecules and the subsequent degradation. Besides, the higher crystallization degree of anatase, the more oxygen vacancies and/or defects, the stronger absorbance for UV lights resulting from the supercritical treatment could also enhance the photocatalytic activity, as discussed above. Furthermore, the supercritical treatment could strengthen the interaction between the La_2O_3 and the TiO_2, which might enhance the promoting effect of the La-modification on the photocatalytic performance. The durability test could further confirm the above conclusion. As shown in Fig. 10, the La/TiO_2-1.25(SC) can be used repetitively for more than eight times without significant decrease in activity. However, the La/TiO_2-1.25(DC) loses 32% activity even after being used for three times. According to ICP analysis, the deactivation of the La/TiO_2-1.25(DC) is mainly attributed to the leaching off of the La-dopants since 37.6% La_2O_3 in the La/TiO_2-1.25(DC) has been leached-off after being used for three times. However, no significant leaching-off of La_2O_3 in the La/TiO_2-1.25(SC) has been observed even after being used for eight times. Thus, one could conclude that the supercritical treatment could enhance the interaction between the La_2O_3 and the TiO_2 and thus inhibit the leaching of the La-dopants, leading to enhanced durability of the La/TiO_2-1.25(SC) in photocatalysis.

(3) The activity of the La/TiO_2-1.25(SC) increases with the calcination temperature increasing from 673 to 773 K, which could be attributed to the increase of the crystallization degree of anatase as shown in Fig. 5. Further increase in the calcination temperature results in the decrease of surface area, leading to the decrease in activity. The optimum calcination temperature is determined as 773 K.

(4) The La/TiO_2-1.25(SC/US) is most active among all the as-prepared undoped and La-doped TiO_2 photocatalysts. Its activity is nearly twice as that of the P25, showing a good potential in practical application. The higher activity of the La/TiO_2-1.25(SC/US) than that of the La/TiO_2-1.25(SC) could be mainly attributed to both the higher particle dispersion owing to the dispersing effect of the ultrasound and the stronger absorbance for UV lights owing to the enhanced interaction between the La_2O_3 and the TiO_2 induced by ultrasonication.

4. Conclusions

In summary, a new approach has been developed to synthesize a highly active La-doped TiO_2 photocatalyst by combining the sol–gel method with both the ultrasonication and the supercritical treatment. The La-modification, the ultrasonication and the treatment under supercritical conditions could increase the particle dispersion, the crystallization degree of anatase, the surface oxygen vacancies and defects, the interaction between the La-dopants and the TiO_2, which might facilitate the adsorption for reactant molecules and UV lights, and also inhibit the recombination between photoelectrons and holes, leading to the higher photocatalytic activity. The present method offers new opportunities for designing more active TiO_2-based and even non-titania photocatalysts which may promote the practical application of photocatalysis in environmental cleaning.

Acknowledgements

This work was supported by the National Natural Science Foundation of China (20377031), Shanghai Leading Academic Discipline Project (T0402), the Science and Technology Ministry of China (2005CCA01100) and Shanghai Municipal Education Commission (06DZ013).

References

[1] L. Zhang, C. Lange, I. Abraham, S. Storck, W.F. Maier, H. Kisch, J. Phys. Chem. B 102 (1998) 10765–10771.
[2] J. Schwitzgebel, J.G. Ekerdt, H. Gerischer, A. Heller, J. Phys. Chem. 99 (1995) 5633–5638.
[3] M.R. Hoffmann, S.T. Martin, W. Choi, D.W. Bahnemann, Chem. Rev. 95 (1995) 69–96.
[4] H. Yamashita, H. Miwa, M. Harada, Y. Ichihashi, M. Anpo, J. Phys. Chem. B 102 (1998) 10707–10711.
[5] X.H. Wang, J.G. Li, H. Kamiyama, Y. Moriyoshi, T. Ishigaki, J. Phys. Chem. B 110 (2006) 6804–6809.
[6] X.Z. Li, F.B. Li, Environ. Sci. Technol. 35 (2001) 2381–2387.
[7] N. Venkatachalam, M. Palanichamy, V. Banumathi Arabindoo, Murugesan, J. Mol. Catal. A 266 (2007) 158–165.
[8] P.N. Kapoor, S. Uma, S. Rodriguez, K.J. Klabunde, J. Mol. Catal. A 229 (2005) 145–150.
[9] S. Sakthivel, M. Janczarek, H. Kisch, J. Phys. Chem. B 108 (2004) 19384–19387.
[10] L.Q. Jing, X.J. Sun, B.F. Xin, B.Q. Wang, W.M. Cai, H.G. Fu, J. Solid State Chem. 177 (2004) 3375–3382.
[11] X.H. Wu, X.B. Ding, W. Qin, W.D. He, Z.H. Jiang, J. Hazard. Mater. B 137 (2006) 192–197.
[12] Sh. Yuan, Q.R. Sheng, J.L. Zhang, F. Chen, M. Anpo, Q.H. Zhang, Microporous Mesoporous Mater. 79 (2005) 93–99.
[13] I. Atribak, I. Such-Basanez, A. Bueno-Lopez, A. Garcia Garcia, Catal. Commun. 8 (2007) 478–482.
[14] R. Gopalan, Y.S. Lin, Ind. Eng. Chem. Res. 34 (1995) 1189–1195.
[15] C.A. Leduc, J.M. Campbell, J.A. Rossin, Ind. Eng. Chem. Res. 35 (1996) 2473–2476.
[16] C.P. Sibu, S. Rajesh Kumar, P. Mukundan, K.G.K. Warrier, Chem. Mater. 14 (2002) 2876–2881.
[17] H.X. Li, J. Zhu, G.S. Li, J. Chem. Lett. 33 (2004) 574–575.
[18] H.X. Li, G.S. Li, J. Zhu, Y. Wan, J. Mol. Catal. 226 (2005) 93–100.
[19] H.X. Li, J.X. Li, Y.N. Huo, J. Phys. Chem. B 110 (2006) 1559–1565.
[20] J.G. Yu, M.H. Zhou, B. Cheng, H.G. Yu, X.J. Zhao, J. Mol. Catal. A 227 (2005) 75–80.
[21] J.C. Yu, L.Z. Zhang, J.G. Yu, Chem. Mater. 14 (2002) 4647–4653.
[22] A. Serret, M.V. Cabanas, R.M. Vallet, Chem. Mater. 12 (2000) 3836–3841.
[23] B.M. Reddy, A. Khan, P. Akshmanan, J. Phys. Chem. B 109 (2005) 3355–3363.
[24] J.C. Parker, R.W. Siegel, Appl. Phys. Lett. 57 (1990) 943–945.
[25] J.G. Yu, J.C. Yu, M.K.P. Leung, W.K. Ho, B. Cheng, X.J. Zhao, J.C. Zhao, J. Catal. 217 (2003) 69–78.
[26] T. Brar, P. France, P.G. Smirniotis, Ind. Eng. Chem. Res. 40 (2001) 1133–1139.
[27] K.S. Suslick, S.B. Choe, A. Cichowlas, M.W. Grinstaff, Nature 353 (1991) 414–416.
[28] P. Mulvaney, M. Cooper, F. Grieser, D. Meisel, J. Phys. Chem. 94 (1990) 8339–8345.